

Estimation of parameters in carbon sequestration models from net ecosystem exchange data

Luther White ^{a,*}, Frances White ^a, Yiqi Luo ^b, Tao Xu ^b

^a *Department of Mathematics, University of Oklahoma, Norman, OK 73019, United States*

^b *Department of Botany and Microbiology, University of Oklahoma, Norman, OK 73019, United States*

Abstract

The use of net ecosystem exchange (NEE) data to estimate carbon transfer coefficients is investigated in the context of a deterministic compartmental carbon sequestration system. Sensitivity and approximation properties are investigated for the underlying model initial value problems. Joint probability distributions are obtained by including NEE data along with corresponding synthetic NEE values generated from the model and are compared with a priori distributions. These distributions are used to estimate individual transfer parameters and to predict future carbon states. Results are compared with those obtained using only a priori information without the benefit of data. Shannon information content is introduced to measure the dependence of results on the lengths of observational intervals and provide an additional indicator of the value added by the inclusion of NEE data.

© 2006 Elsevier Inc. All rights reserved.

Keywords: Net ecological exchange; Inversion; Information content

1. Introduction

Observed net ecosystem exchange (NEE) of carbon reflects a fine balance between canopy photosynthetic carbon influx into and respiratory efflux out of an ecosystem. To quantify terrestrial carbon sinks, the biosphere–atmosphere interactions research community has employed the eddy-covariance technique to measure NEE, water, and energy in more than 210 sites worldwide [1]. Approximately 1000 site years of NEE data and millions of data points have been accumulated from the FluxNet measurements. Consequently, it appears that the eddy-flux database will increase exponentially in the coming years and will become a great resource for ecological research. Flux data, for example, have been used to estimate the components of net ecosystem productivity (NEP, i.e., carbon sinks/sources) at many of the flux sites [7], to validate ecosystem models [2,8,10] and to characterize diurnal, seasonal, and interannual patterns [6]. It will continue to be a fruitful yet challenging task for the research community to exploit this massive database to improve our mechanistic understanding and predictive knowledge of ecosystem processes [5,16].

* Corresponding author.

E-mail address: lwhite@ou.edu (L. White).

The present work focuses on the utilization of NEE data and seeks to investigate its usefulness in the estimation of parameters within a compartmental carbon sequestration model. Previously we have used other data sets that are less extensive than NEE [17]. The objective in this paper is to give a proper mathematical formulation for the use of this data in a compartmental model, to compare the information added using NEE data over a priori constraints, to assess the effect on carbon predictions based on NEE data with those using a priori constraints, and to determine the information value of time series observations of NEE as a function of the length of the observational interval.

In this work our analysis is within framework of an underlying compartmental model with seven carbon pools in which scaling factors along with initial conditions and flux distribution terms are known to various extents. We view the model as a deterministic initial value problem in which environmental and flux terms are presented as approximations of observed time series. Hence, we view certain coefficients as deterministic time dependent functions and are interested in the stability of results when those functions are perturbed. The parameters to be estimated belong to an admissible set Q_{ad} prescribed by a priori bounds. Initially, it is assumed that all parameters in the admissible set are equally likely. Hence a uniform distribution designated as the homogeneous distribution is defined on the sample space Q_{ad} . A posteriori distributions resulting from the incorporation of NEE data are obtained and are then compared with this a priori homogeneous distribution [15].

Information on parameters may be deduced by means of various operations on the resulting joint probability density function (pdf). The first such operation is marginalization to obtain a cumulative distribution function (cdf) of individual parameters. While initially flux and initial conditions are assumed known, the effect of uncertainty in these parameters is also included. A measure of the information provided by data is to compare corresponding probability intervals between the a priori and the a posteriori marginal distributions for parameters. A further comparison is to compare a priori and a posteriori predicted distributions of pool sizes. In this comparison we wish to assess the effect that the inclusion of data has on the cdf of predicted likely pool sizes. Finally, we use the notion of Shannon relative information content to compare the effect of data.

From the perspective taken here, data is associated with an observational NEE mapping that takes the system state to a data space where measurements are made. Our interest is to use the model and data to investigate the information associated with this mapping. Our approach is to use the model to generate simulated data by specifying vectors of admissible parameters. By solving the model equations we obtain associated states. Synthetic NEE output is then constructed by applying the observational operator to this state. Comparing the synthetic NEE data with observed NEE data, we then generate a joint pdf on the set of admissible parameters. This pdf contains a priori information on the parameters as well as the information from the data. From this pdf we calculate marginal pdfs, likelihood intervals, and estimators. We may then compare estimators based on our procedure with the generating parameter.

In Section 2, we pose the underlying model as a deterministic initial value problem and indicate in detail the assumptions on various coefficients. Differentiability, stability, approximation, and convergence results are discussed that are important for the analysis of the problem. In Section 3, the NEE operator is defined. Its differentiability and sensitivity properties with respect to perturbations of parameters are observed. The observational NEE data is also introduced. In Section 4, the a posteriori joint pdf function based on NEE data is given. A posteriori distributions of carbon transfer coefficients are obtained and compared with the a priori homogeneous distributions. In addition, distributions of predicted pools sizes based on the NEE data are presented. Finally, results are presented that includes various degrees of uncertainty in flux and initial value distributions. In Section 5, Shannon information content is used and viewed as a function of the length of the observation time interval to determine the value added of additional data as a function of the measurement time. Information efficiency is also introduced as the ratio of information per unit time to use as an indicator of the value of information.

2. Underlying system and approximation

In this work, we consider a seven compartment model in which the state of various carbon pools at time t is expressed in terms of a column 7-vector $\mathbf{x}(t)$ the components of which represent the quantity of material per square meter of nonwoody biomass, woody biomass, metabolic litter, structural litter, microbes, slow organic matter, and passive organic matter pools [17], respectively. The passage of carbon among these pools is modelled by an initial value problem

$$\frac{d}{dt}\mathbf{x}(t) = \xi(t)A_o C\mathbf{x}(t) + \mathbf{b}u(t) \quad \text{for } t \in (0, T], \quad (2.1)$$

$$\mathbf{x}(0) = \mathbf{x}_0. \quad (2.2)$$

The matrix C is a 7×7 diagonal matrix whose entries consist of the components of a vector \mathbf{c}

$$C = \text{diag}(\mathbf{c})$$

of coefficients modelling the transfer of carbon among the various pools. The coefficients satisfy bounds

$$0 \leq c_i \leq c_i^{\max}$$

for $i = 1, \dots, 7$, where the vector of upper bounds on the transfer parameters is given by

$$\mathbf{c}^{\max} = \begin{bmatrix} 0.004 \\ 0.0003 \\ 0.03 \\ 0.002 \\ 0.02 \\ 1.5 \times 10^{-4} \\ 4.0 \times 10^{-6} \end{bmatrix}. \quad (2.3)$$

Bounds given in \mathbf{c}^{\max} are posed in [17–19]. Initially, we take the set Q_{ad} of admissible parameters to be given by

$$Q_{\text{ad}} = \{\mathbf{c} : 0 \leq c_i \leq c_i^{\max}\}.$$

It is also of interest to allow the vectors \mathbf{b}_o and \mathbf{x}_o to vary. Thus, we define bounds on the flux partitioning vector \mathbf{b} of the form

$$\begin{aligned} \mathbf{b}^{\max} &= (1 + b_{\text{pert}})\mathbf{b}_o, \\ \mathbf{b}^{\min} &= (1 - b_{\text{pert}})\mathbf{b}_o \end{aligned} \quad (2.4)$$

and on the initial conditions \mathbf{x}_o of the form

$$\begin{aligned} \mathbf{x}_o^{\max} &= (1 + x_{\text{pert}})\mathbf{x}_o, \\ \mathbf{x}_o^{\min} &= (1 - x_{\text{pert}})\mathbf{x}_o, \end{aligned} \quad (2.5)$$

where the vectors \mathbf{b}_o and \mathbf{x}_o are given by

$$\mathbf{b}_o = \begin{bmatrix} 0.25 \\ 0.30 \\ 0 \\ 0 \\ 0 \\ 0 \\ 0 \end{bmatrix} \quad (2.6)$$

and

$$\mathbf{x}_o = \begin{bmatrix} 469 \\ 4100 \\ 64 \\ 694 \\ 123 \\ 1385 \\ 923 \end{bmatrix}, \quad (2.7)$$

respectively. The bounds x_{pert} and b_{pert} are assumed to be zero initially so that $\mathbf{b} = \mathbf{b}_0$ and $\mathbf{x}_0 = \mathbf{x}_0$. However, we will later include results allowing x_{pert} and b_{pert} to take on various values. In this case the admissible set of parameters includes not only values for the transfer coefficients \mathbf{c} but also the flux distribution vector \mathbf{b} and initial values \mathbf{x}_0 .

The vector $\mathbf{x}(t)$ represents the density of carbon in grams per square meter in each pool at time t . The 7×7 matrix A gives interaction weights among the various pools. The matrix A_0 is given by

$$A_0 = \begin{bmatrix} -1 & 0 & 0 & 0 & 0 & 0 & 0 \\ 0 & -1 & 0 & 0 & 0 & 0 & 0 \\ 0.712 & 0 & -1 & 0 & 0 & 0 & 0 \\ 0.288 & 1 & 0 & -1 & 0 & 0 & 0 \\ 0 & 0 & 0.45 & 0.275 & -1 & 0.42 & 0.45 \\ 0 & 0 & 0 & 0.275 & 0.296 & -1 & 0 \\ 0 & 0 & 0 & 0 & 0.004 & 0.03 & -1 \end{bmatrix} \tag{2.8}$$

and describes the partitioning of carbon among the pools.

Environmental effects are modelled by means of a scalar-valued function $t \mapsto \zeta(t)$, cf [10] that we now discuss. The environmental function depends on temperature and moisture effects. The temperature effects are modelled through a temperature-dependent function

$$\tau(t) = T(\hat{\tau}(t)), \tag{2.9}$$

where

$$t \mapsto \hat{\tau}(t) = 14.8 + 14 \sin\left(\frac{2\pi(t + 266)}{365}\right) \tag{2.10}$$

is a function approximating the actual temperature time series [9] see Fig. 1.

The function τ is expressed by

$$\tau(t) = T(\hat{\tau}(t)) = (0.65)2.2^{(\hat{\tau}(t)-10)/10} \tag{2.11}$$

see [11].

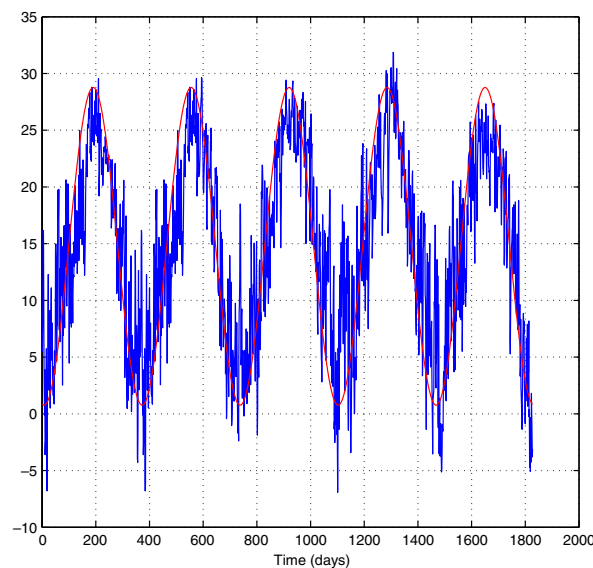


Fig. 1. Temperature time series with approximation.

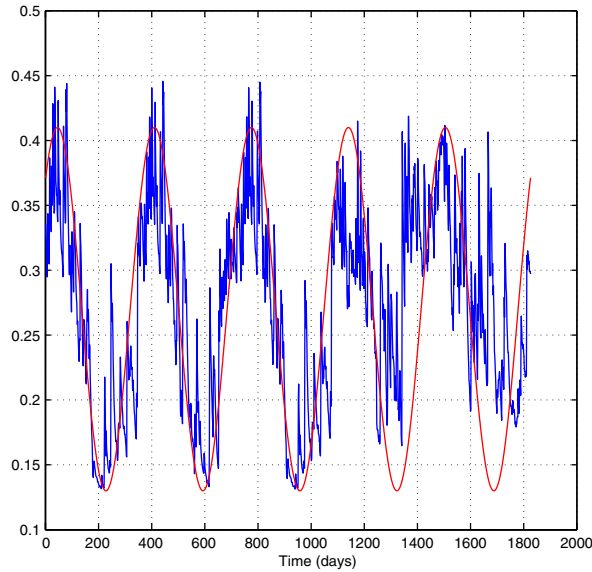


Fig. 2. Moisture time series with approximation.

The environmental function is also dependent on a function that captures moisture effects. The moisture time series and its approximating function is portrayed in Fig. 2. The approximating function is

$$\hat{m}(t) = 0.27 + 0.14 \sin\left(\frac{2\pi(t + 46)}{365}\right). \tag{2.12}$$

The moisture model function m is expressed by

$$m(t) = M(\hat{m}(t)) = \begin{cases} 5\hat{m}(t) & \text{when } \hat{m}(t) < 0.2, \\ 1 & \text{otherwise.} \end{cases} \tag{2.13}$$

The environmental modelling function [11] is now given as the product

$$\xi(t) = \tau(t) \times m(t) = T(\hat{\tau}(t)) \times M(\hat{m}(t)). \tag{2.14}$$

We note that the temperature model T is differentiable with respect to the temperature function $\hat{\tau}$. The moisture model M is Lipschitz continuous with respect to the moisture function \hat{m} and satisfies

$$|M(\hat{m}_1(t)) - M(\hat{m}_2(t))| \leq 5|\hat{m}_1(t) - \hat{m}_2(t)|$$

for each $t \in [0, T]$. Hence, it follows that the function ξ is only Lipschitz continuous with respect to t .

The carbon flux time series is portrayed in Fig. 3 and is approximated [9] by the function

$$u(t) = 8 + 7 \sin\left(\frac{2\pi(t + 269)}{365}\right). \tag{2.15}$$

The functions ξ and u all are periodic of the same period 365 and bounded. We also note that daily readings are available for approximately 5 years. Denote a common bound for ξ and u by K so that

$$|\xi(t)| \leq K$$

and

$$|u(t)| \leq K$$

for all $t \in [0, T]$. Also, denote by \bar{c} the bound on the parameters $\mathbf{c} \in Q_{ad}$ so that

$$|\mathbf{c}| \leq \bar{c}$$

for all $\mathbf{c} \in Q_{ad}$.

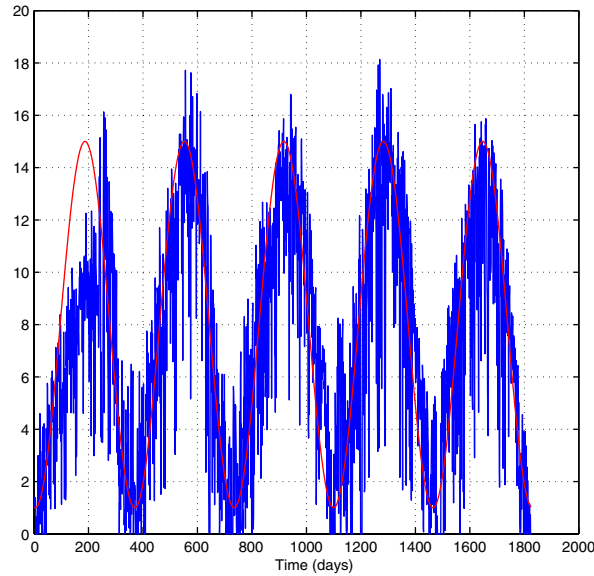


Fig. 3. Carbon flux time series with approximation.

Given the approximations of the temperature, moisture, and flux time series, the continuous behavior of solutions of the model equation with respect to perturbation of problem parameters such as ξ , u , \mathbf{x}_0 , A_0 , \mathbf{c} , and \mathbf{b} is critical. Standard estimates may be applied using classical Gronwall arguments [4]. For example, consider the initial value problem

$$\begin{aligned} \frac{d}{dt} \mathbf{x}(t) &= A(t)\mathbf{x}(t) + \mathbf{B}(t), \\ \mathbf{x}(0) &= \mathbf{x}_0, \end{aligned}$$

in which the entries of the matrix $A(t)$ and the vector $\mathbf{B}(t)$ are continuous real-valued functions defined on $[0, T]$. Let α and β be positive real numbers such that

$$\|A(t)\| \leq \alpha$$

and

$$\|\mathbf{B}(t)\| \leq \beta$$

for all $t \in [0, T]$, where the vector norm is the Euclidean norm on \mathfrak{R}^7 and the matrix norm is the Frobenius norm [13]. It follows that for all $t \in [0, T]$ that:

$$\|\mathbf{x}(t)\| \leq \|\mathbf{x}_0\|e^{\alpha t} + \frac{\beta}{\alpha}(e^{\alpha t} - 1)$$

and

$$\left\| \frac{d}{dt} \mathbf{x}(t) \right\| \leq e^{\alpha t}(\alpha \|\mathbf{x}_0\| + \beta).$$

Set $q = (A, \mathbf{B}, \mathbf{x}_0)$ and denote dependence of \mathbf{x} on q by $\mathbf{x}(q)$. Taking the variations q' to consist of perturbations of A and \mathbf{B} by continuous functions A' and \mathbf{B}' and of the vector \mathbf{x}'_0 , differentiability of the function $q \mapsto \mathbf{x}(q)$ follows from results in [3] and the Fréchet derivative satisfies:

$$\begin{aligned} \frac{d}{dt} [D\mathbf{x}(q)q'](t) &= A(t)[D\mathbf{x}(q)q'](t) + A'(t)\mathbf{x}(q)(t) + \mathbf{B}'(t), \\ [D\mathbf{x}(q)q'](0) &= \mathbf{x}'_0. \end{aligned}$$

It follows then that:

$$\|\mathbf{x}(q + q')(t) - \mathbf{x}(q)(t)\| \leq K_0 \|q'\|$$

and

$$\left\| \frac{d}{dt} \mathbf{x}(q + q')(t) - \frac{d}{dt} \mathbf{x}(q)(t) \right\| \leq K_1 \|q'\|,$$

where the constants K_0 and K_1 are independent of $q \in Q$, where Q is a set of parameters that are bounded in the suitable spaces.

Remark 2.1. Initially, for the system (2.1) and (2.2), we are interested only in perturbations with respect to the parameter \mathbf{c} with \mathbf{b}_o and \mathbf{x}_0 constant. However, the above indicates that these results are stable with respect to changes in \mathbf{b}_o and \mathbf{x}_0 and ζ and u .

The bound for the solution $\mathbf{x}(t)$ is given by

$$|\mathbf{x}(\mathbf{c})(t)| \leq \left(|\mathbf{x}_0| + \frac{|\mathbf{b}|}{|A_o| \bar{c}} \right) e^{|A_o| \bar{c} T} - \frac{|\mathbf{b}|}{|A_o| \bar{c}}. \tag{2.16}$$

Remark 2.2. From the previous discussion, the Fréchet differentiability of the solution of (2.1) and (2.2) with respect to \mathbf{c} , \mathbf{b} , and \mathbf{x}_0 , follows from classical results, see [3]. Fréchet differentiability with respect to the functions ζ and u also are immediate. However, because of the Lipschitz continuity of ζ with respect to \hat{m} , only Lipschitz continuity of the solution with respect to \hat{m} holds. The Fréchet derivative of the stat \mathbf{x} with respect to \mathbf{c} satisfies the equation

$$\frac{d}{dt} [D\mathbf{x}(\mathbf{c})] = \zeta(t) A_o \{ C [D\mathbf{x}(\mathbf{c})] + \text{diag}(\mathbf{x}(\mathbf{c})) \}. \tag{2.17}$$

Remark 2.3. The differentiability with respect to the above parameters along with the Lipschitz continuity of M with respect to \hat{m} implies the continuous dependence of the solution \mathbf{x} with respect to \hat{c} , \hat{m} , and u as well as \mathbf{c} , \mathbf{x}_0 , and \mathbf{b} .

A simple Euler’s method is used for approximation. The difference equations are obtained with $h = T/N$ as

$$\frac{\mathbf{x}_{j+1} - \mathbf{x}_j}{h} = A_o C \zeta_j \mathbf{x}_j + \mathbf{b} u_j$$

with iteration

$$\mathbf{x}_{j+1} = [I + h A_o C \zeta_j] \mathbf{x}_j + h \mathbf{b} u_j \tag{2.18}$$

for $j = 0, 1, \dots, N - 1$.

Remark 2.4. Under assumptions of continuity for the functions ζ and u , classical approximation results [14] show that solutions of the difference approximations converge to the solution of the initial value problem (2.1)–(2.5) uniformly with respect to parameters in Q_{ad} . The global convergence rate is of order $O(h)$ because the environmental function $t \mapsto \zeta(t)$ is only Lipschitz continuous and not differentiable. However, because of the form of M and the moisture function $t \mapsto m(t)$, higher order results hold for time subintervals.

Remark 2.5. From the above, the differentiability of (2.7) is straight forward. For example, the derivative with respect to \mathbf{c} is given by

$$[D_c \mathbf{x}]_{j+1} = [I + h A_o C] [D_c \mathbf{x}]_j + h A_o \text{diag}(\mathbf{x}_j).$$

We refer to [17–19] for other formulas and adjoint equations expressing the derivatives.

3. The NEE observation operator and data

NEE measurements indicate the change in the total carbon of the system per unit time. From these measurements we wish to obtain information of the transfer coefficients \mathbf{c} . Accordingly, setting

$$\phi = [1 \ 1 \ 1 \ 1 \ 1 \ 1 \ 1]^*$$

where the superscript * denotes vector transpose, the observational model for NEE is given by

$$N(\mathbf{c})(t) = \frac{d}{dt} \phi^* \mathbf{x}(\mathbf{c})(t).$$

In terms of the system (2.1)–(2.5) it is convenient to express the NEE operator as

$$N(\mathbf{c})(t) = \phi^* [\xi(t) A_0 C \mathbf{x}(\mathbf{c})(t) + \mathbf{b}u(t)].$$

A similar formula holds for the finite difference approximation

$$N(\mathbf{c})_i = \phi^* [\xi_i A_0 C \mathbf{x}(\mathbf{c})_i + \mathbf{b}u_i].$$

To obtain a measure of the sensitivity of NEE to perturbations of the parameter \mathbf{c} , we consider the derivative of $\mathbf{c} \mapsto N(\mathbf{c})(t)$ expressed by the row vector

$$D_c N(\mathbf{c})(t) = \xi(t) \phi^* A_0 [C D_c \mathbf{x}(\mathbf{c})(t) + \text{diag}(\mathbf{x}(\mathbf{c})(t))]$$

with the corresponding expression for the discrete case

$$D_c N(\mathbf{c})_i = \xi_i \phi^* A_0 [C D_c \mathbf{x}(\mathbf{c})_i + \text{diag}(\mathbf{x}(\mathbf{c})_i)].$$

Since

$$N(\mathbf{c}_0 + \mathbf{c}')(t) - N(\mathbf{c}_0)(t) \approx [D_c N(\mathbf{c}_0)(t)] \mathbf{c}',$$

it follows that:

$$V(\mathbf{c}, \mathbf{c}')(t) = |N(\mathbf{c}_0 + \mathbf{c}')(t) - N(\mathbf{c}_0)(t)|^2 \approx \mathbf{c}'^* [D_c N(\mathbf{c}_0)(t)]^* [D_c N(\mathbf{c}_0)(t)] \mathbf{c}'$$

with the obvious corresponding discrete expression. In Fig. 4, the graphs of the mapping $t \mapsto V(\mathbf{c}, \mathbf{c}')(t)$ are represented for the case in which $\mathbf{c}' = \mathbf{c}_{\max}$ with $T = 1830$. Taking the $L^2(0, T)$ norm of $V(\mathbf{c}, \mathbf{c}')$ of each of the partial derivatives yields the vector,

$$\text{Global sensitivity} = [0.78, 0.30, 0.06, 0.39, 0.27, 0.12, 0.0039].$$

This indicates that NEE is sensitive to perturbations in the parameters $c_1, c_4, c_2, c_5, c_6, c_3,$ and c_7 in that order.

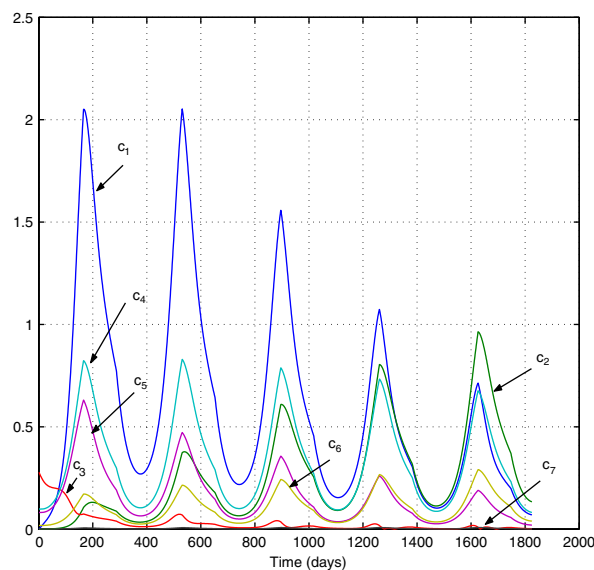


Fig. 4. Comparison of NEE operator sensitivities.

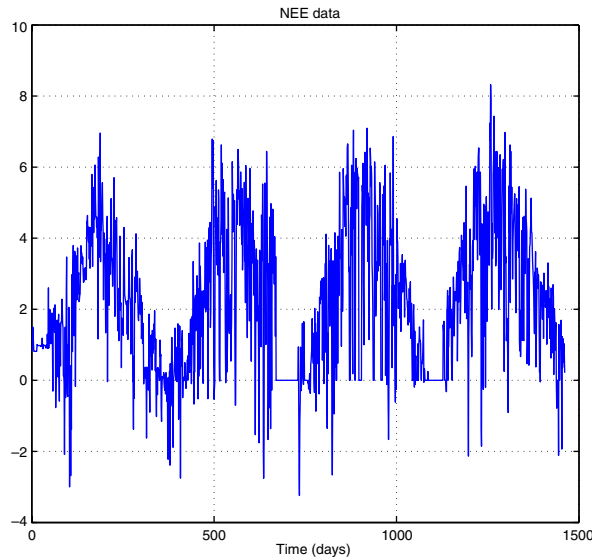


Fig. 5. NEE 98 data.

The NEE data that we use is portrayed in Fig. 5. It is notable that daily data is available over a 4 year period with the exception of a couple of gaps.

4. The joint probability density function, marginalization, reduction of likelihood intervals

We introduce the fit-to-data functional in the continuous case as the usual quadratic criterion

$$J(\mathbf{c}) = \frac{1}{2} \int_0^T [N(\mathbf{c})(t) - N_o(t)]^2 dt \tag{4.1}$$

to measure the distance NEE output associated with a transfer coefficient vector \mathbf{c} is from data $N_o(t)$. In our application since there are gaps in the data we introduce the discrete functional, again using $J(\mathbf{c})$,

$$J(\mathbf{c}) = \frac{1}{2} \sum_{i=1}^{N_{\text{obs}}} (N(\mathbf{c})_{j_i} - N_{o_i})^2. \tag{4.2}$$

The sum is over those times t_{j_i} at which measurements are available. Thus, the fit-to-data functional is defined over the set of admissible parameters Q_{ad} described in (2.3)–(2.7) and assigns an error between a simulated NEE function $N(\mathbf{c})_{j_i}$ associated with a parameter \mathbf{c} and the observed data values $\{N_{o_i} : i = 1, \dots, N_{\text{obs}}\}$. At this point it is assumed that $x_{\text{pert}} = 0$ and $b_{\text{pert}} = 0$. We introduce a probability density function (pdf) by introducing the function

$$f(\mathbf{c}) = \hat{C} \exp[-J(\mathbf{c})]. \tag{4.3}$$

Using this approach we may introduce probabilistic notions to interpret results in addition to the minimization approach used in least squares estimation [17–19]. Hence, the parameter space Q_{ad} is a sample space over which f is defined. The constant \hat{C} is a normalization constant used to scale the pdf to unity over Q_{ad} . By integrating f over subsets of Q_{ad} we obtain the probability that parameters belong to those subsets given the data. We also think of functions of the sample parameters as random variables defined over Q_{ad} . The pdf contains all the information in the problem from the data, the model, and the a priori constraints. Our objective is to assess the information added to our knowledge based on the data. In this work we consider how likelihood intervals of parameters are reduced by comparing the corresponding marginalized a posteriori

pdfs with the a priori pdfs. These comparisons yield information on how our knowledge of the value of the parameters has increased by including data.

Our second measure is to consider the pool size distributions predicted based on a posteriori distribution joint pdf as compared with the predictions without the benefit of the data based on the a priori information. Since NEE data is available for approximately four years and the approximating time series for temperature, moisture, and CO₂ flux is over five years (in fact can be extended indefinitely using the functional forms), we also make predictions of future NEE values.

Having formed the joint pdf f defined on Q_{ad} , the task remains to extract information contained in the joint pdf concerning the parameters. In this work we use randomly generated simulations and compare the associated NEE with the data. Since we are interested in the comparison with a priori distributions without the benefit of the data, we retain all simulated values. Thus, we do not use Markov Chain Monte Carlo (MCMC) methods [12] to capture those parameters of most significance.

In Fig. 6 is portrayed the marginalized cdfs for $c_1, c_2, c_4,$ and c_5 and in Fig. 7 for $c_3, c_6,$ and c_7 . The 20–80 likelihood ratios determined from marginal cumulative distributions with the benefit of data and without are the following for c_1-c_7 :

$$\text{Likelihood ratio } (20, 80) = [0.5, 0.96, 0.8, 0.65, 0.72, 0.93, 1.0].$$

Note that the likelihood is substantially reduced for the coefficients $c_1, c_4, c_5,$ and c_3 . In this study, there very little gained in the estimation of $c_2, c_6,$ and c_7 . The correlation coefficient between the likelihood ratio (20,80) and the global sensitivity is -0.83 . This indicates a strong negative correlation between the likelihood ratios and the sensitivity coefficients calculated previously.

Fig. 8 portrays the cdfs for predicted pool sizes for $x_1, x_2, x_3,$ and x_4 and Fig. 9 portrays $x_5, x_6,$ and x_7 . We note that there are reductions in spread for $x_1, x_3,$ and x_4 . For x_6 and x_7 the intervals are shifted while the additional data does not effect x_2 and x_5 .

The above results assume a fixed known value for the flux distribution vector, \mathbf{b} , and the initial condition vector, \mathbf{x}_0 . The stability results in Section 2 indicate the differentiability of solutions of the model equations and of the NEE operator with respect to \mathbf{b} and \mathbf{x}_0 . As an experiment we allowed errors in \mathbf{b} and \mathbf{x}_0 by adjusting b_{pert} and x_{pert} in setting bounds on \mathbf{b} and \mathbf{x}_0 . Results for c_1 and x_1 are portrayed in Figs. 10 and 11. These figures indicate again that results are stable with respect to perturbations. However, as to be expected, results vary substantially as the magnitude of the perturbations is allowed to increase.

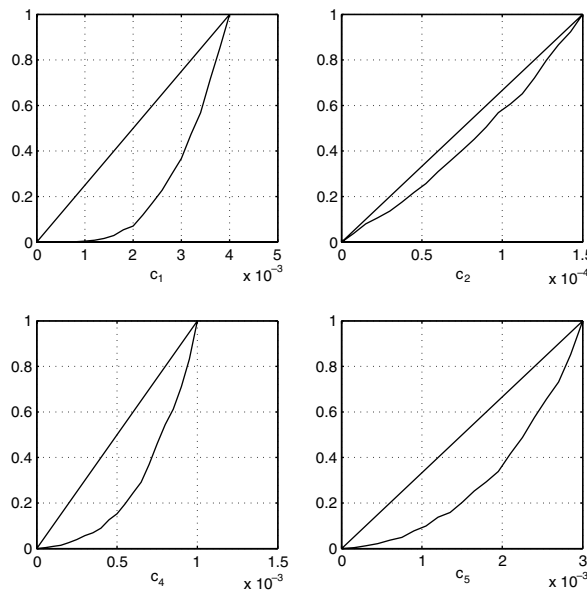


Fig. 6. Marginal cumulative distribution functions for $c_1, c_2, c_4,$ and c_5 in 1/days .

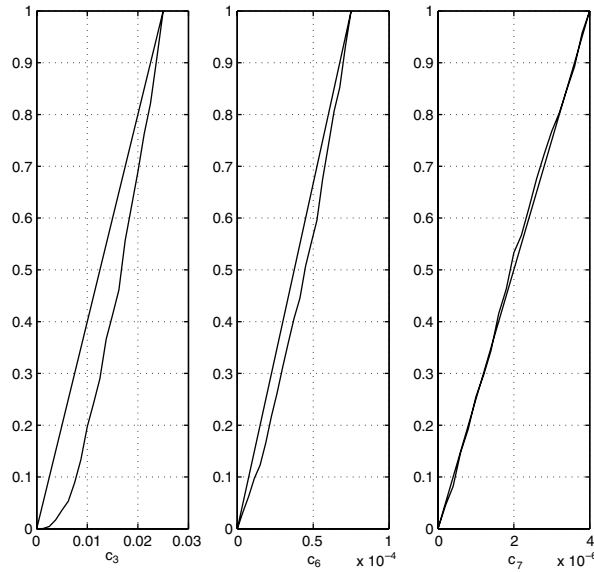


Fig. 7. Marginal cumulative distribution functions for c_3 , c_6 , and c_7 in 1/days.

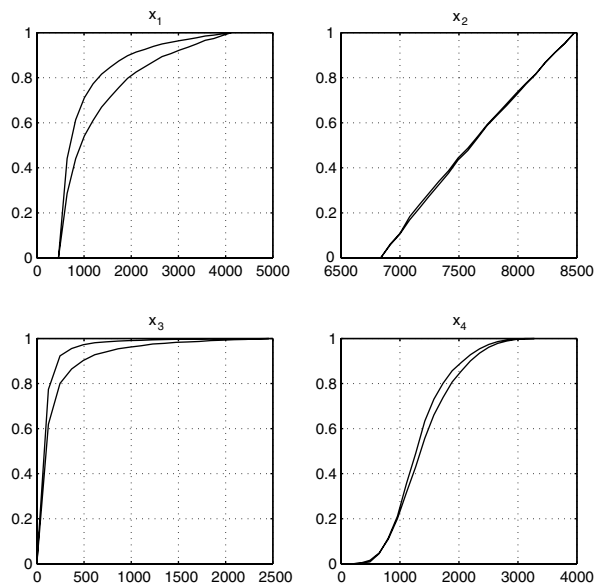


Fig. 8. Marginal cumulative distribution functions for x_1 , x_2 , x_3 , and x_4 in g/cm^2 .

5. Information content and dependence on observation interval length

In the previous section, an entire data set of NEE observations is used. In this section, we investigate the dependence of results on observation interval length, T . It is convenient to introduce the notion of Shannon’s relative information content. Denote the a priori distribution by $\mathbf{c} \mapsto \pi(\mathbf{c})$. For the purposes of this work we take π to be uniform distribution defined over Q_{ad} . It is again assumed that \mathbf{b} and \mathbf{x}_0 are known exactly. The information content [15] of the a posteriori joint distribution $\mathbf{c} \mapsto f(\mathbf{c})$ relative to the uniform distribution is given by

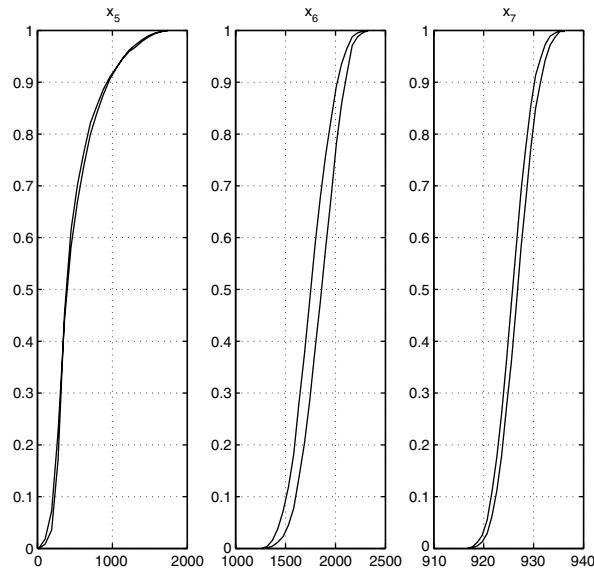


Fig. 9. Marginal cumulative distribution functions for x_5 , x_6 , and x_7 in g/cm^2 .

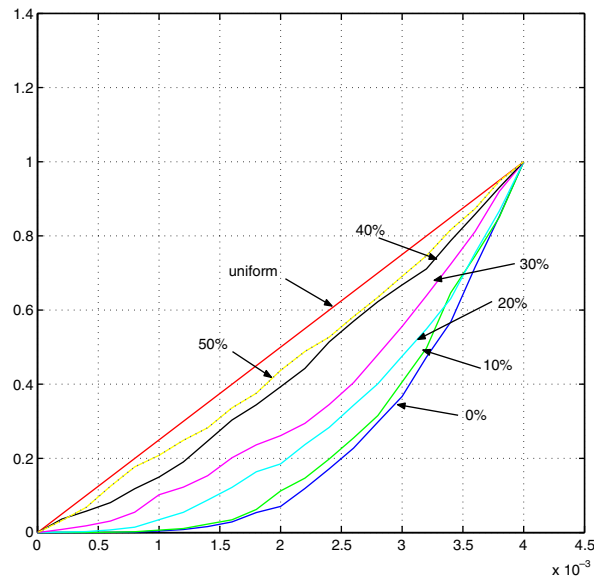


Fig. 10. Comparison of c_1 marginal cdfs with errors in \mathbf{b}_0 and \mathbf{x}_0 in 1/days.

$$I = \int_{Q_{\text{ad}}} f(\mathbf{c}) \log \left(\frac{f(\mathbf{c})}{\pi(\mathbf{c})} \right) d\mathbf{c}. \tag{5.1}$$

Since we are interested in relative values and the distribution $\mathbf{c} \mapsto \pi(\mathbf{c})$ is a constant over Q_{ad} , we consider

$$I = \int_{Q_{\text{ad}}} f(\mathbf{c}) \log(f(\mathbf{c})) d\mathbf{c}. \tag{5.2}$$

Recall that

$$J(\mathbf{c}; T) = \frac{1}{2} \int_0^T (N(\mathbf{c})(t) - N_o(t))^2 dt, \tag{5.3}$$

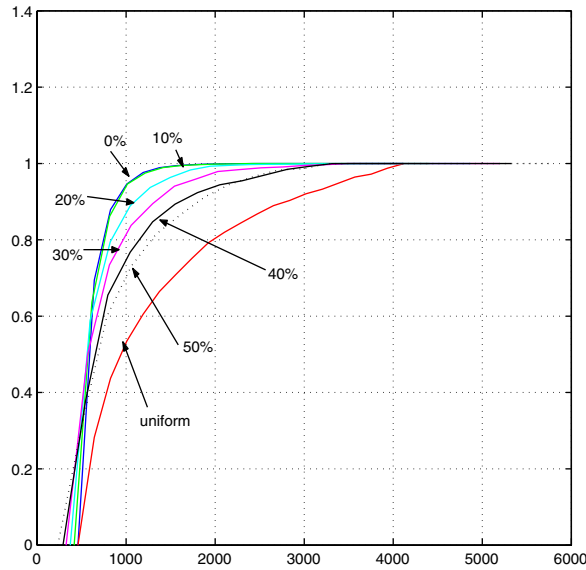


Fig. 11. Comparison of x_1 marginal cdfs with errors in b_0 and x_0 in g/cm^2 .

where N_o is a time dependent function of observed values and where we include dependence of the fit-to-data functional on the length of the observation interval T . The joint pdf is defined as

$$f(\mathbf{c}; T) = K(T) \exp[-J(\mathbf{c}; T)] \tag{5.4}$$

with

$$K(T) = \left\{ \int_{Q_{ad}} \exp[-J(\mathbf{c}; T)] d\mathbf{c} \right\}^{-1}. \tag{5.5}$$

It is clear that relative information content depends on T , and we indicate this dependence by

$$I(T) = \int_{Q_{ad}} f(\mathbf{c}; T) \log(f(\mathbf{c}; T)) d\mathbf{c}.$$

The differentiability is clear, and the derivative with respect to T may be calculated. We begin by noting that

$$\frac{\partial}{\partial T} J(\mathbf{c}; T) = \frac{1}{2} [N(\mathbf{c})(T) - N_o(T)]^2. \tag{5.6}$$

It easily follows that:

$$\frac{d}{dT} K(T) = \frac{1}{2} K(T)^2 \int_{Q_{ad}} \exp[-J(\mathbf{c}; T)] [N(\mathbf{c})(T) - N_o(T)]^2 d\mathbf{c}$$

so that

$$\frac{d}{dT} K(T) = \frac{1}{2} K(T) \int_{Q_{ad}} f(\mathbf{c}; T) [N(\mathbf{c})(T) - N_o(T)]^2 d\mathbf{c}. \tag{5.7}$$

Set

$$\bar{V}(T) = \int_{Q_{ad}} f(\mathbf{c}; T) [N(\mathbf{c})(T) - N_o(T)]^2 d\mathbf{c}$$

so that

$$\frac{d}{dT} K(T) = \frac{1}{2} K(T) \bar{V}(T). \tag{5.8}$$

Continuing, we find

$$\frac{\partial}{\partial T} f(\mathbf{c}, T) = f(\mathbf{c}, T) \{ \bar{V}(T) - [N(\mathbf{c})(T) - N_o(T)]^2 \}. \tag{5.9}$$

Finally, differentiating $I(T)$ and using Eqs. (5.3)–(5.9), we have

$$\frac{d}{dT} I(T) = \int_{Q_{ad}} \{ 1 + \log[f(\mathbf{c}, T)] \} f(\mathbf{c}, T) \{ \bar{V}(T) - [N(\mathbf{c})(T) - N_o(T)]^2 \} d\mathbf{c}.$$

Noting that

$$\int_{Q_{ad}} f(\mathbf{c}, T) \{ \bar{V}(T) - [N(\mathbf{c})(T) - N_o(T)]^2 \} d\mathbf{c} = 0,$$

we then obtain

$$\frac{d}{dT} I(T) = \bar{V}(T) I(T) - \int_{Q_{ad}} f(\mathbf{c}, T) \log[f(\mathbf{c}, T)] [N(\mathbf{c})(T) - N_o(T)]^2 d\mathbf{c} \tag{5.10}$$

establishing an expression for the derivative of the information content.

In Fig. 12, the solid curve indicates the computed relative information content as a function of the percentage of the data set that is used. Under the assumption that as T increases the variance of the error decreases to zero, we consider the differential equation with $p > 1$

$$\frac{d}{dT} I(T) = \alpha T^{-p} (I(T) - \beta), \tag{5.11}$$

where α and β are positive constants. The solution of this equation is given by

$$I(T) = \beta + \text{Const} \exp \left[-\alpha \frac{T^{p-1}}{p-1} \right]. \tag{5.12}$$

The dashed curve in Fig. 12 is a solution of the differential equation (5.12) with parameters

$$\alpha = 5, \quad \beta = 0.35, \quad p = 1.295, \quad \text{and} \quad \text{Const} = 1.$$

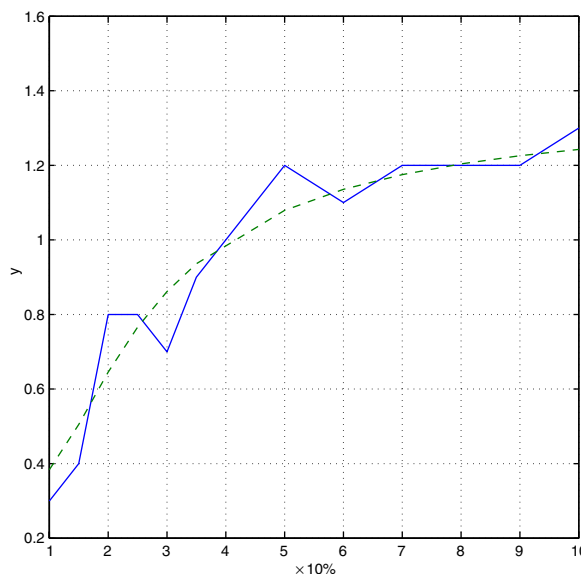


Fig. 12. Comparison of observed and modelled relative information content.

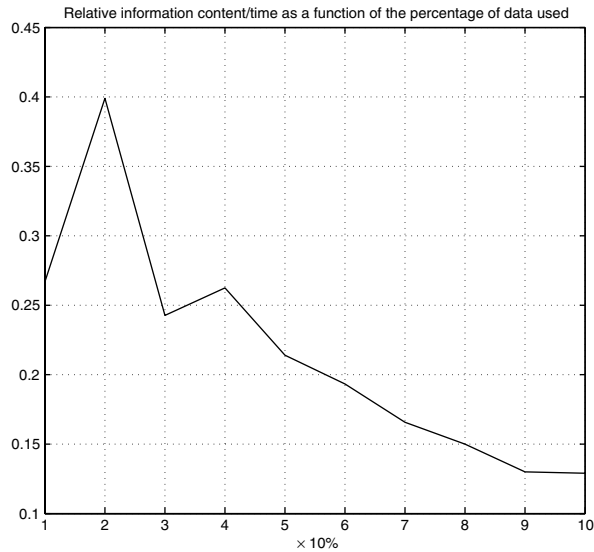


Fig. 13. Relative information content as a function of the percent of the data record.

The relative information content increases monotonically as an increasing percentage of the data set used. This is to be expected. However, the rate of increase appears to diminish. One would expect that, with the presence of noise in the measurements, information would not increase indefinitely.

Finally, we consider the information per unit time as an indicator of the information per unit cost. Thus, function $I(T)/T$ gives the information per unit time and may be considered as a measure of information efficiency. Of course, any function of cost could be used. The division by T is only used as an illustration. Fig. 13 indicates a maximum relatively early in the observation period with decreasing data efficiency after as time evolves. Certainly, data over longer periods is useful, however the relative increase is most dramatic at earlier times when there is little information.

6. Conclusions

We have provided a formulation for the estimation of transfer parameters in a carbon sequestration model using NEE data. The underlying compartmental model is introduced as an initial value problem with approximations to the environmental and flux terms. Stability of system solutions with respect to perturbations of those terms is demonstrated along basic approximation, differentiability and convergence results. Introducing the NEE observational mapping taking system states to the corresponding NEE values, sensitivity indicators are obtained for the NEE observational mapping with respect to transfer parameters from differentiability properties. It is observed that the model-based NEE mapping is globally sensitive to transfer coefficients associated with nonwoody biomass, structural litter, woody biomass, microbes, slow organic matter, metabolic litter, and passive organic matter in decreasing order. Using randomly generated parameter values along with the NEE data, marginal pdfs are obtained for individual transfer parameters. The resulting likelihood interval ratios are strongly negatively correlated with sensitivity coefficients and indicate reductions in nonwoody biomass, structural litter, microbes, metabolic litter, slow organic matter, woody biomass, and passive organic matter from largest reduction to smallest. Also, cumulative distributions of predicted carbon pool sizes indicate reduced uncertainty with the inclusion of NEE data. In particular, the likelihood intervals are reduced for predicted nonwoody biomass, metabolic litter, and structural litter pools using NEE data. Finally, we consider the dependence of relative information content on the length of the observational interval. The derivative of information content with respect to the observational interval length is obtained. Under the assumption that variance of the error goes to zero as T^{-p} with $p > 1$ where T denotes the length of the observation time interval, we obtain good fit with observed results. Numerical results indicate increasing information with increasing

time; however, at a decreasing rate. Moreover, the efficiency of the data has a maximum. A combination of these results could be utilized in considering the length of the observation time interval.

Acknowledgements

This study was financially supported by the Office of Science (BER), US Department of Energy, Grant No. DE-FG03-99ER62800. This research is also part of the Forest-Atmospheric Carbon Transfer and Storage (FACTS-1) project at the Duke Forest. The FACTS-1 project is supported by the US Department of Energy, Office of Biological and Environmental Research, under DOE contract DE-FG05-95ER62083 at Duke University and contract DE-AC02-98CH10886 at Brookhaven National Laboratory.

References

- [1] D.D. Baldocchi, Assessing the eddy covariance technique for evaluating carbon dioxide exchange rates of ecosystems: past, present and future, *Global Change Biol.* 9 (2003) 479–492.
- [2] K.L. Clark, W.P. Cropper, H.L. Gholz, Evaluation of modeled carbon fluxes for a slash pine ecosystem: SPM2 simulations compared to eddy flux measurements, *Forest Sci.* 47 (2001) 52–59.
- [3] J. Dieudonne, *Foundations of Modern Analysis*, Academic Press, New York, 1960.
- [4] G. Duvaut, J.L. Lions, *Inequalities in Mechanics and Physics*, Springer-Verlag, New York, 1976.
- [5] M.L. Goulden, J.W. Munger, S.M. Fan, B.C. Daube, S.C. Wofsy, Exchange of carbon dioxide by a deciduous forest: response to inter-annual climate variability, *Science* 271 (1996) 1576–1578.
- [6] D. Hui, Y. Luo, G. Katul, Partitioning inter-annual variability in net ecosystem exchange between climatic variability and function changes, *Tree Physiol.* 23 (2003) 433–442.
- [7] A.S. Kowalski, M. Sartore, R. Burrell, P. Berbigier, D. Loustau, The annual carbon budget of a French pine forest (*Pinus pinaster*) following harvest, *Global Change Biol.* 9 (7) (2003) 1051–1065.
- [8] B.E. Law, M. Williams, P.M. Anthoni, et al., Measuring and modeling seasonal variation of carbon dioxide and water vapour exchange of a *Pinus ponderosa* forest subject to soil water deficit, *Global Change Biol.* 6 (6) (2000) 613–630.
- [9] D.G. Luenberger, *Optimization by Vector Space Methods*, Wiley, New York, 1969.
- [10] Y. Luo, B. Medlyn, D. Hui, D. Ellsworth, J. Reynolds, G. Katul, Gross primary productivity in Duke forest: modeling synthesis of CO₂ experiment and eddy-flux data, *Ecol. Appl.* 11 (2001) 239–252.
- [11] Y.L. Luo, L. White, J. Canadell, E. DeLucia, D. Ellsworth, A. Finzi, J. Lichten, W. Schlesinger, Sustainability of terrestrial carbon sequestration: a case study in Duke Forest with an inversion approach, *Global Biogeochem. Cycles* 17 (1) (2003).
- [12] C. Robert, G. Casella, *Monte Carlo Statistical Methods*, Springer, New York, 1999.
- [13] G. Stewart, *Introduction to Matrix Computations*, Academic Press, New York, 1973.
- [14] J. Stoer, R. Burlisch, *Numerical Analysis*, Springer-Verlag, New York, 1980.
- [15] A. Tarantola, *Inverse Problem Theory*, SIAM, Philadelphia, 2005.
- [16] R. Valentini, G. Matteucci, A.J. Dolman, et al., Respiration as the main determinant of European forests carbon balance, *Nature* 404 (2000) 861–865.
- [17] L. White, Y. Luo, Model-based assessment for terrestrial carbon processes: implications for sampling strategies in FACE experiments, *Appl. Math. Comput.* 167 (2005) 419–434.
- [18] L. White, Y. Luo, T. Xu, Carbon sequestration: inversion of FACE data and prediction, *Appl. Math. Comput.* 166 (2005) 783–800.
- [19] L. White, Y. Luo, Estimation of carbon transfer coefficients using Duke Forest free-air CO₂ enrichment data, *Appl. Math. Comput.* 130 (2002) 101–120.